ChemComm

COMMUNICATION

View Article Online
View Journal

Cite this: DOI: 10.1039/d6cc01930g

Received 30th March 2026,
Accepted 18th May 2026

DOI: 10.1039/d6cc01930g

rsc.li/chemcomm

Double-shelled hollow iron-encapsulated zeolite for enhanced mass transfer and reusability in persulfate activation

Qibo Liu,[ac] Wei Pang,[b] Xiaohan Chen,[c] Pinli Diao,[c] Wen Tian,[ab] Feng Cui,[a] Yide Han, *[a] Huanying Zhou *[b] and Sibudjing Kawi *[c]

A double-shelled hollow iron-encapsulated zeolite (Fe_2O_3@H-ZSM-5@H-ZSM-5) catalyst was synthesized *via* a stepwise etching–recrystallization strategy for persulfate activation. The unique double-shelled hollow architecture enhances mass transfer while ensuring ultra-low iron leaching and excellent structural stability, resulting in outstanding reusability.

Antibiotics and dyes have been frequently detected in environmental waters due to their widespread use in medical, livestock farming and industrial applications.[1,2] Their high chemical stability and poor biodegradability enable persistence and accumulation, posing ecological risks and potential threats to human health.[3,4] Conventional treatment technologies often fail to achieve complete removal, thereby motivating the development of more powerful oxidative remediation approaches.[5,6]

Persulfate-based advanced oxidation processes (PS-AOPs) have emerged as effective routes for degrading persistent organic pollutants, owing to their broad pH tolerance, low catalyst demand, and high redox potential of sulfate radicals ($SO_4^{\bullet-}$).[7] Persulfate activation can be achieved *via* photochemical,[8] thermal,[9] ultrasonic,[10] electrochemical,[11] and transition-metal-mediated pathways.[12] Among these, iron-based catalysts are promising for efficient reactive oxygen species (ROS) generation during persulfate activation. However, homogeneous iron activation typically requires acidic conditions and suffers from difficult recovery and secondary sludge generation, limiting practical applications.[13] Accordingly, heterogeneous iron-based catalysts, such as supported catalysts,[14] mixed metal oxide catalysts,[15] and doping-modified catalysts,[16] have been extensively explored. Nevertheless, leaching of iron species and their poor reusability remain major challenges.

Zeolites are regarded as promising supports for iron species owing to their excellent hydrothermal stability, well-defined microporous structures, and molecular sieving effects.[17] The confinement effect of zeolitic frameworks can enhance the dispersion of iron species during crystallization and effectively suppress iron leaching under catalytic conditions.[18] However, the intrinsically long and narrow micropore channels impose diffusion limitations on PDS and short-lived ROS, resulting in sluggish degradation kinetics. Several strategies, such as creating hollow or hierarchical zeolite architectures, can shorten diffusion pathways and enhance mass transfer.[19] However, etching-induced shell defects may compromise structural integrity, resulting in increased leaching of iron species and their poor reusability.

Double-shelled hollow zeolites possess unique advantages, including shortened diffusion pathways, enhanced mechanical stability, and enlarged surface area. These are beneficial for improving mass transfer and catalytic performance.[20] Recently, multi-/double-shelled hollow zeolites have been applied in several catalytic reactions, including hydrocarbon conversion,[21] methanol aromatization,[22] and hydrodeoxygenation processes.[23] Although templating[21] and defect-etching strategies[23] have been reported for constructing double-shelled hollow zeolites, the controllable construction of multi-shelled hollow zeolites with well-confined active sites remains highly desirable. Moreover, their application remains largely unexplored in the PS-AOPs field, particularly for simultaneously enhancing mass transfer and achieving excellent reusability.

Herein, we report a double-shelled hollow iron-encapsulated zeolite (Fe_2O_3@H-ZSM-5@H-ZSM-5) catalyst synthesized *via* a stepwise etching–recrystallization strategy for PDS activation. We come to a conclusion that (i) the confinement effect of ZSM-5 promotes the uniform dispersion and stabilization of iron species, (ii) the hollow architecture enhances the mass transfer of PDS and ROS, and (iii) the robust double-shelled structure

[a] *Department of Chemistry, College of Sciences, Northeastern University, Shenyang, 110819, P. R. China. E-mail: hanyide@mail.neu.edu.cn*
[b] *Tianjin Key Laboratory of Risk Assessment and Control Technology for Environment and Food Safety, Military Medical Sciences Academy, Academy of Military Sciences, Tianjin 300050, China. E-mail: zhouhytj@163.com*
[c] *Department of Chemical and Biomolecular Engineering, National University of Singapore, 4 Engineering Drive 4, 117585, Singapore. E-mail: chekawis@nus.edu.sg*

ensures ultra-low iron species leaching and excellent structural stability, enabling outstanding reusability. More importantly, the proposed stepwise etching–recrystallization strategy provides an alternative approach for constructing multi-shelled hollow catalysts and may inspire the design of other multi-shelled hollow-structured catalytic systems.

A schematic illustration of the synthetic route for Fe_2O_3@H-ZSM-5@H-ZSM-5 is shown in Fig. 1a. The catalyst was constructed *via* a stepwise etching–recrystallization strategy, which integrates hydrothermal crystallization, controlled etching, and secondary shell growth. First, Fe species were introduced into ZSM-5 *via* impregnation to form Fe_2O_3/ZSM-5. Subsequently, controlled alkaline etching was employed to generate the hollow Fe_2O_3@H-ZSM-5. Then, secondary crystallization was carried out to sequentially grow an S-1 intermediate layer and an outer ZSM-5 shell. Finally, a second alkaline treatment was applied to synthesize the double-shelled hollow Fe_2O_3@H-ZSM-5@H-ZSM-5 catalyst. Detailed synthetic procedures are provided in the supplementary information (SI).

As shown in Fig. 1b, all catalysts exhibit characteristic diffraction peaks corresponding to the MFI structure, indicating the successful formation of the ZSM-5 framework in all samples. Notably, no characteristic diffraction peaks of Fe_2O_3 are observed for Fe_2O_3/ZSM-5 and Fe_2O_3@H-ZSM-5@H-ZSM-5, which may be attributed to the high dispersion or ultra-fine size of Fe_2O_3 species with crystallite sizes below the detection limit of XRD.[24] The morphology and size of the as-prepared samples were observed by SEM, as shown in Fig. 1c. Both ZSM-5 (c1) and Fe_2O_3/ZSM-5 (c2) exhibit a typical disc-like morphology with an average diameter of ~250 nm and a thickness of ~160 nm. Moreover, no obvious Fe_2O_3 aggregates are observed on the surface of Fe_2O_3/ZSM-5. In contrast, Fe_2O_3@H-ZSM-5@H-ZSM-5 (c3) displays an ellipsoidal morphology with a larger particle size of ~300 nm, which may be associated with repeated shell growth during the multi-step synthesis processes. As shown in Fig. 1d, both ZSM-5 (d1) and Fe_2O_3/ZSM-5 (d2) exhibit a totally solid structure. However, Fe_2O_3 clusters with a size of ~9 nm can be clearly observed in Fe_2O_3/ZSM-5, suggesting that the ZSM-5 framework effectively confines the growth of Fe_2O_3 species.

Furthermore, SEM and TEM images of Fe_2O_3@H-ZSM-5 can be found in Fig. S1 (SI). Moreover, Fe_2O_3@H-ZSM-5@H-ZSM-5 displays a well-defined double-shelled hollow structure. The inner cavity has a size of ~180 nm × 110 nm with an inner shell thickness of ~20 nm, while the outer cavity is ~30 nm with an outer shell thickness of ~14 nm, and the overall particle size is ~300 nm × 210 nm, confirming the successful construction of the double-shelled hollow architecture. In addition, no obvious Fe_2O_3 clusters are observed on the surface of Fe_2O_3@H-ZSM-5@H-ZSM-5, which may be attributed to the partial migration or loss of iron species during the alkaline etching process, leading to a higher dispersion of the remaining iron species. Furthermore, elemental mapping (Fig. 1e) shows that Si, Al, O, and Fe are uniformly distributed throughout Fe_2O_3@H-ZSM-5@H-ZSM-5. The proportion of the main elements in different samples is listed in Table S1 (SI). ZSM-5 possesses a Si/Al ratio of 42.95, which is favorable for the formation of the hollow structure. For Fe_2O_3/ZSM-5, the Si/Al ratio exhibits a slight change, and the iron content is determined to be 4.49 wt%. In contrast, the Si/Al ratio of Fe_2O_3@H-ZSM-5@H-ZSM-5 increases to 67.51, which is likely related to the repeated shell growth and alkaline etching during the multi-step synthesis processes. Meanwhile, the iron content decreases to 0.90 wt%. Overall, these results confirm the successful construction of Fe_2O_3@H-ZSM-5@H-ZSM-5 with a double-shelled hollow structure.

Tetracycline (TC) was selected as a representative organic pollutant, and the degradation conditions were optimized as shown in Fig. S2 (SI). The optimal degradation conditions were determined as follows: pH 5, 15 mg of Fe_2O_3@H-ZSM-5@H-ZSM-5, and 30 mg of PDS. As shown in Fig. 2, only 35.2% of TC was removed using the Fe_2O_3/ZSM-5/PDS system within 150 min, with a reaction rate constant (k_{obs}) of 0.00335 min^{-1}. This relatively low activity may be attributed to the diffusion limitation of PDS and ROS within the microporous channels of

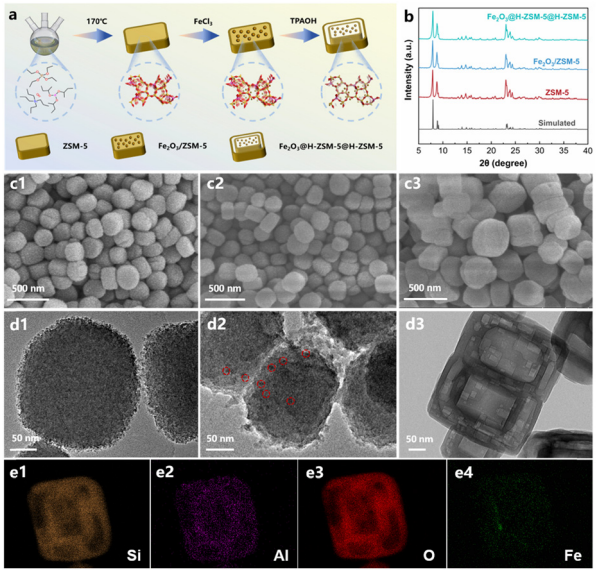

Fig. 1 (a) A schematic illustration of the synthetic route for Fe_2O_3@H-ZSM-5@H-ZSM-5. (b) XRD patterns of as-prepared samples. SEM images of (c1) ZSM-5, (c2) Fe_2O_3/ZSM-5, and (c3) Fe_2O_3@H-ZSM-5@H-ZSM-5. TEM images of (d1) ZSM-5, (d2) Fe_2O_3/ZSM-5, and (d3) Fe_2O_3@H-ZSM-5@H-ZSM-5. (e) Elemental distribution of Fe_2O_3@H-ZSM-5@H-ZSM-5.

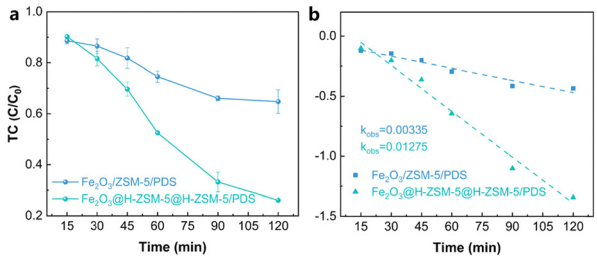

Fig. 2 (a) The TC degradation efficiencies and (b) the values of k_{obs} in different degradation systems.

ZSM-5. In contrast, 73.9% of TC was removed using the Fe_2O_3@H-ZSM-5@H-ZSM-5/PDS system, with a k_{obs} value of 0.01275 min^{-1}. Notably, despite the lower iron loading (0.90 wt%), the k_{obs} value is still approximately four times higher than that of the Fe_2O_3/ZSM-5/PDS system. Quantitative calculation further reveals that the utilization efficiency of iron species in Fe_2O_3@H-ZSM-5@H-ZSM-5 is about 20 times higher than that in Fe_2O_3/ZSM-5. This significant improvement can be attributed to the hollow structure of Fe_2O_3@H-ZSM-5@H-ZSM-5, which facilitates the mass transfer of PDS and ROS and shortens the diffusion pathways during the catalytic reaction.

Electron paramagnetic resonance (EPR) spectroscopy was employed to identify the ROS generated in the Fe_2O_3@H-ZSM-5@H-ZSM-5/PDS system. As shown in Fig. 3a, strong signals of DMPO-$^{\bullet}$OH, DMPO-$^{\bullet}O_2^-$, and TEMP-$^1O_2$, together with a relatively weak DMPO-$SO_4^{\bullet-}$ signal, can be clearly observed, indicating the involvement of multiple ROS ($^{\bullet}$OH, $SO_4^{\bullet-}$, $^{\bullet}O_2^-$, and $^1O_2$) in TC degradation. To further quantify the contribution of each ROS, 100 mM MeOH, 100 mM TBA, 5 mM p-BQ, and 10 mM FFA were added to the reaction system as ROS scavengers.[25] As shown in Fig. 3b and c, the addition of p-BQ only slightly affects the TC degradation efficiency, with a removal rate of 66.00%. In contrast, the addition of FFA significantly suppresses the TC degradation, while the value of k_{obs} decreases from 0.01275 min^{-1} to 0.00169 min^{-1}. The contribution rates of individual ROS were further quantitatively calculated, as shown in Fig. 3d. Among the ROS, $SO_4^{\bullet-}$ exhibits a relatively significant contribution rate of 28.01%, highlighting the advantage of PDS as an oxidant. Meanwhile, $^1O_2$ plays a major role, with a contribution rate of 52.13%, which is consistent with the quenching experiment results.[26] Furthermore, as shown in Fig. 3e, iron species in the fresh Fe_2O_3@H-ZSM-5@H-ZSM-5 mainly exist in the form of Fe_2O_3. During the PDS activation process, iron species act as the main active sites, and approximately 53.07% of Fe(III) is reduced to Fe(II). Based on these results, a possible catalytic mechanism is proposed: PDS is activated by the iron species in Fe_2O_3@H-ZSM-5@H-ZSM-5 to generate multiple ROS, while a portion of Fe(III) is reduced to Fe(II). Among the ROS, $^1O_2$ plays the predominant role during the TC degradation process.

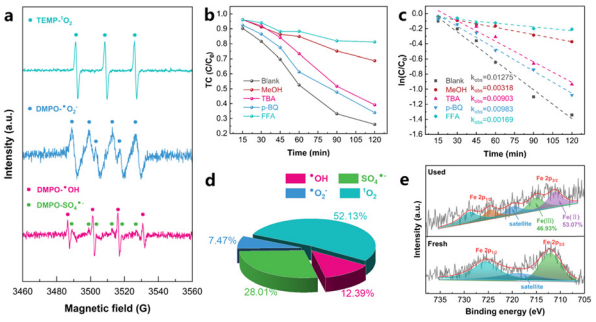

Fig. 3 (a) EPR spectra in the Fe_2O_3@H-ZSM-5@H-ZSM-5/PDS system. (b) TC degradation efficiencies and (c) the values of k_{obs} in the presence of various scavengers. (d) Contribution rate of each ROS during the TC degradation process. (e) XPS spectra of Fe 2p of fresh and spent Fe_2O_3@H-ZSM-5@H-ZSM-5.

The leaching of iron species, structural stability, and reusability of Fe_2O_3@H-ZSM-5@H-ZSM-5 were systematically investigated. The iron species leaching concentration after each reaction was determined using a modified 1,10-phenanthroline method.[27] As shown in Fig. 4a, the iron species leaching concentration after the first cycle is only 0.011 mg L^{-1}, which decreases to below the detection limit after four cycles. Furthermore, the iron species leaching concentration of Fe_2O_3@H-ZSM-5@H-ZSM-5 was compared with those of previously reported catalysts. As shown in Fig. 4b, the iron species leaching concentration of Fe_2O_3@H-ZSM-5@H-ZSM-5 is significantly lower than that reported in most literature studies, and the detailed comparison is shown in Table S2 (SI). This result indicates that the double-shelled structure of Fe_2O_3@H-ZSM-5@H-ZSM-5 effectively suppresses the leaching of iron species during the catalytic process due to its double-shell barrier effect. Moreover, the spent catalyst was characterized by XRD (Fig. 4c) and SEM (Fig. S3). The results show that the catalyst still retains the characteristic MFI structure after repeated reactions. Meanwhile, its particle size and morphology show only slight changes, and no obvious structural damage or surface cavities are observed, indicating that Fe_2O_3@H-ZSM-5@H-ZSM-5 possesses excellent structural stability, which is attributed to its robust double-shelled structure. More importantly, the reusability of Fe_2O_3@H-ZSM-5@H-ZSM-5 was tested. As shown in Fig. 4d, after eight consecutive cycles, the TC degradation efficiency decreases by only 8.2% compared with the initial run, demonstrating the outstanding reusability. Overall, the unique double-shelled hollow architecture of Fe_2O_3@H-ZSM-5@H-ZSM-5 not only effectively suppresses the leaching of iron species, but also ensures excellent structural stability, resulting in outstanding reusability during the TC degradation process. Additional practical application evaluation, including catalyst-loaded membrane performance,

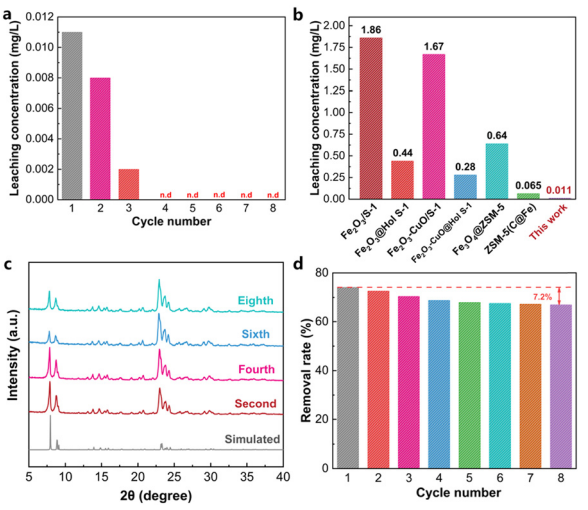

Fig. 4 (a) Iron species leaching concentration after each catalytic cycle. (b) Comparison of iron species leaching concentrations. (c) XRD patterns of the spent Fe_2O_3@H-ZSM-5@H-ZSM-5 catalyst. (d) TC removal rate during repeated catalytic cycles.

anti-interference capability, and real water treatment tests, is provided in the SI.

In this work, a double-shelled hollow iron-encapsulated zeolite (Fe_2O_3@H-ZSM-5@H-ZSM-5) catalyst was successfully synthesized *via* a stepwise etching–recrystallization strategy. Benefiting from the hollow architecture, the value of k_{obs} in the Fe_2O_3@H-ZSM-5@H-ZSM-5/PDS system is approximately 4 times higher than that in the Fe_2O_3/ZSM-5/PDS system. More importantly, owing to its robust double-shelled structure, Fe_2O_3@H-ZSM-5@H-ZSM-5 exhibits an ultra-low iron leaching concentration (0.011 mg L^{-1}) and excellent structural stability, which together endow the catalyst with outstanding reusability, as evidenced by only a slight decrease (8.2%) in TC removal rate after eight consecutive cycles. This stepwise etching–recrystallization strategy provides an alternative approach for constructing multi-shelled hollow catalysts and may inspire the design of other multi-shelled hollow-structured catalysts for AOPs and water purification.

Qibo Liu: writing – original draft, methodology, investigation, formal analysis, and data curation. Wei Pang: methodology, investigation, formal analysis, and data curation. Xiaohan Chen: methodology, investigation, and formal analysis. Pinli Diao: methodology, investigation, and funding acquisition. Wen Tian: methodology, investigation, formal analysis, conceptualization, and data curation. Feng Cui: writing – original draft, methodology, investigation, formal analysis, data curation, and validation. Yide Han: writing – review & editing, investigation, funding acquisition, formal analysis, conceptualization, and project administration. Huanying Zhou: investigation, funding acquisition, formal analysis, and conceptualization. Sibudjing Kawi: writing – review & editing, formal analysis, conceptualization, data curation, funding acquisition, and supervision.

Conflicts of interest

There are no conflicts to declare.

Data availability

Data supporting the findings of this study are available within the article and its supplementary information (SI). Supplementary information is available. See DOI: https://doi.org/10.1039/d6cc01930g.

Additional data are available from the corresponding author upon reasonable request.

Acknowledgements

This work was supported by the National Natural Science Foundation of China (grant: 21771032) and the China Scholarship Council (CSC).

References

1 Z. Chen, G. Meng, Z. Han, H. Li, S. Chi, G. Hu and X. Zhao, *J. Colloid Interface Sci.*, 2025, **679**, 67–78.
2 Y. Li, M. Wang, X. Chen, S. Cui, N. Hofstra, C. Kroeze, L. Ma, W. Xu, Q. Zhang, F. Zhang and M. Strokal, *Water Res.*, 2022, **209**, 117906.
3 S. M. Zainab, M. Junaid, N. Xu and R. N. Malik, *Water Res.*, 2020, **187**, 116455.
4 J. Li, D. Wang, S. Zhao, R. Ma, J. Guo, Z. Li, D. Wang, Y. Xuan and L. Wang, *Appl. Catal., B*, 2024, **351**, 124007.
5 A. Raichur and N. Sinha, *Sep. Purif. Technol.*, 2023, **308**, 122830.
6 H. Xiong, S. Dong, J. Zhang, D. Zhou and B. Rittmann, *Water Res.*, 2018, **136**, 75–83.
7 P. Koundle, N. Nirmalkar and G. Boczkaj, *J. Environ. Chem. Eng.*, 2025, **374**, 124107.
8 M. Amasha, A. Baalbaki and A. Ghauch, *Chem. Eng. J.*, 2018, **350**, 132323.
9 Y. Zhou, Y. Xiang, Y. He, Y. Yang, J. Zhang, L. Luo, H. Peng, C. Dai, F. Zhu and L. Tang, *J. Hazard. Mater.*, 2018, **359**, 396–407.
10 R. Yin, W. Guo, H. Wang, J. Du, X. Zhou, Q. Wu, H. Zheng, J. Chang and N. Ren, *Chem. Eng. J.*, 2018, **335**, 145–153.
11 S. Yan, X. Zhang and H. Zhang, *J. Hazard. Mater.*, 2019, **374**, 92–100.
12 X. Zheng, X. Niu, D. Zhang, M. Lv, X. Ye, J. Ma, Z. Lin and M. Fu, *Chem. Eng. J.*, 2022, **429**, 132323.
13 S. Xiao, M. Cheng, H. Zhong, Z. Liu, Y. Liu, X. Yang and Q. Liang, *Chem. Eng. J.*, 2020, **384**, 123265.
14 Y. Zhang, B. Zhang, Y. Teng, J. Zhao and X. Sun, *J. Hazard. Mater.*, 2021, **401**, 123428.
15 L. Fang, K. Liu, F. Li, W. Zeng, Z. Hong, L. Xu, Q. Shi and Y. Ma, *J. Hazard. Mater.*, 2021, **403**, 123669.
16 Z. Jin, Y. Li, H. Dong, S. Xiao, J. Xiao, D. Chu, X. Hou, S. Xiang, Q. Dong and L. Li, *Chem. Eng. J.*, 2022, **448**, 137620.
17 H. Chi, J. Wan, Y. Ma, Y. Wang, M. Huang, X. Li and M. Pu, *J. Hazard. Mater.*, 2020, **398**, 123024.
18 Q. Liu, Y. Wang, X. Sang, J. Bi, N. Liu, X. Zhang, Z. Wang and Y. Han, *Sep. Purif. Technol.*, 2025, **354**, 129369.
19 Q. Liu, J. Bi, Z. Zhai, W. Tian, N. Liu, X. Zhang, Z. Wang, H. Zhou and Y. Han, *J. Environ. Chem. Eng.*, 2025, **13**, 118409.
20 H. Yang, X. Liu, G. Lu and Y. Wang, *Microporous Mesoporous Mater.*, 2026, **225**, 144–153.
21 J. Xiao, K. Cheng, X. Xie, M. Wang, S. Xing, Y. Liu, T. Hartman, D. Fu, K. Bossers, M. A. Huis, A. Blaaderen, Y. Wang and B. M. Weckhuysen, *Nat. Mater.*, 2022, **21**, 572–579.
22 Q. Ma, T. Fu, Z. Wang, C. Li, X. Wu, N. Yang and Z. Li, *Small*, 2024, **20**, 2308502.
23 G. Chen, P. She, J. Han, J. Li, G. Tian, Y. Sun, Y. Gao, G. Yang, Z. Diao, B. Guan and J. Yu, *Angew. Chem., Int. Ed.*, 2025, **64**, e202424690.
24 S. Andonova, S. Tamm, C. Montreuil, C. Lambert and L. Olsson, *Appl. Catal., B*, 2016, **180**, 775–787.
25 J. Qu, Y. Xu, X. Zhang, M. Sun, Y. Tao, X. Zhang, G. Zhang, C. Ge and Y. Zhang, *Appl. Catal., B*, 2025, **316**, 121639.
26 X. Zou, J. Wang, G. Lv, T. Wang, C. Zhou, Y. Chen, J. Shen, S. Su and Z. Liu, *Micropor. Mesopor. Mat.*, 2023, **360**, 112735.
27 C. Adán, A. Bahamonde, I. Oller, S. Malato and A. Martínez-Arias, *Appl. Catal., B*, 2014, **144**, 269–276.

